Measurements of the magnetic field induced by a turbulent flow of liquid metal[a)]

M. D. Nornberg, E. J. Spence, R. D. Kendrick, C. M. Jacobson, and C. B. Forest[b)]
Department of Physics, University of Wisconsin-Madison, 1150 University Avenue, Madison, Wisconsin 53706

(Received 28 October 2005; accepted 20 January 2006; published online 8 May 2006)

Initial results from the Madison Dynamo Experiment provide details of the inductive response of a turbulent flow of liquid sodium to an applied magnetic field. The magnetic field structure is reconstructed from both internal and external measurements. A mean toroidal magnetic field is induced by the flow when an axial field is applied, thereby demonstrating the omega effect. Poloidal magnetic flux is expelled from the fluid by the poloidal flow. Small-scale magnetic field structures are generated by turbulence in the flow. The resulting magnetic power spectrum exhibits a power-law scaling consistent with the equipartition of the magnetic field with a turbulent velocity field. The magnetic power spectrum has an apparent knee at the resistive dissipation scale. Large-scale eddies in the flow cause significant changes to the instantaneous flow profile resulting in intermittent bursts of nonaxisymmetric magnetic fields, demonstrating that the transition to a dynamo is not smooth for a turbulent flow. © *2006 American Institute of Physics*.
[DOI: 10.1063/1.2173614]

I. BACKGROUND

The generation of magnetic fields by flowing electrically conducting fluids is a long-standing problem in plasma physics, astrophysics, and geophysics. Of particular interest is the role of turbulence in either supporting, or suppressing, magnetic fields. Dynamos have been created in the laboratory by driving helical flows of liquid metal through pipes.[1,2] Measurements of the onset of magnetic field growth agree with predictions from laminar theory, suggesting that turbulence played little role in these experiments. The pipe geometry, however, limits the development of eddies to the width of the pipe, a scale much smaller than the device size, thereby inhibiting dynamics due to large-scale turbulence. Since astrophysical flows lack this scale separation, understanding the role of large-scale turbulence is especially important in modeling the dynamo. The Madison Dynamo Experiment was built to characterize these dynamics.

The experiment, shown in Fig. 1, uses two impellers to generate a double-vortex flow of liquid sodium in a 1 m diam spherical vessel. Liquid sodium is used because of its high conductivity ($\sigma=10^7\ \Omega^{-1}\ \mathrm{m}^{-1}$). The choice of a spherical geometry is motivated by the computational work of Dudley and James, which demonstrated that simple time-stationary vortices can generate magnetic fields at relatively low speeds.[3] The flow has been measured in hydrodynamic experiments and is predicted by laminar dynamo theory to generate a transient magnetic field[4] by a slow-dynamo mechanism that stretches and twists magnetic field lines to regenerate the initial seed field.[5] Due to the low kinematic viscosity ($\nu=7\times10^{-5}\ \mathrm{m}^2/\mathrm{s}$), and hence low Prandtl number of liquid sodium ($\mathrm{Pr}\equiv\mu_0\sigma\nu=9\times10^{-4}$), and the large magnetic Reynolds numbers required for spontaneous field growth ($\mathrm{Rm}\equiv\mu_0\sigma LV_0\sim10^2$), the flows required for a dynamo are extremely turbulent ($\mathrm{Re}\equiv LV_0/\nu=\mathrm{Rm}/\mathrm{Pr}\sim10^5$). These types of flows are also studied in experiments at Maryland[6] and Cadarache.[7] The open geometry of these experiments provides the opportunity to study the role of large-scale turbulence in magnetic field generation.

The purpose of this correspondence is to provide a description of the Madison Dynamo Experiment and to report the initial measurements of the magnetic field induced by the flowing liquid metal. The theory of laminar kinematic dynamos and hydrodynamic measurements of the flow are reviewed in Sec. II. The experimental apparatus and its diagnostics are described in Sec. III. Measurements of the mean magnetic field induced when an external magnetic field is applied to the turbulent flow are compared to predictions from the laminar theory in Sec. IV. Measurements of the magnetic field fluctuations are used to study the properties of magnetohydrodynamic (MHD) turbulence in Sec. V.

II. THE KINEMATIC DYNAMO

A. Theory

The evolution of the magnetic and velocity fields in an incompressible conducting fluid is governed by the magnetic induction equation and Navier-Stokes equation with a Lorentz forcing term:

$$\frac{\partial\mathbf{B}}{\partial t}=\boldsymbol{\nabla}\times\mathbf{v}\times\mathbf{B}+\frac{1}{\mu_0\sigma}\boldsymbol{\nabla}^2\mathbf{B}, \tag{1}$$

$$\rho\frac{d\mathbf{v}}{dt}=\mathbf{J}\times\mathbf{B}-\boldsymbol{\nabla}p+\rho\nu\boldsymbol{\nabla}^2\mathbf{v}, \tag{2}$$

where μ_0 is the vacuum magnetic permeability, σ is the fluid conductivity, ρ is the fluid density, and ν is the kinematic viscosity. The time scale for magnetic diffusion is

[a)]Paper BI2 1, Bull. Am. Phys. Soc. **50**, 21 (2005).
[b)]Invited speaker. Electronic mail: cbforest@wisc.edu

 © 2006 American Institute of Physics

Downloaded 08 May 2006 to 128.104.49.126. Redistribution subject to AIP license or copyright, see http://pop.aip.org/pop/copyright.jsp

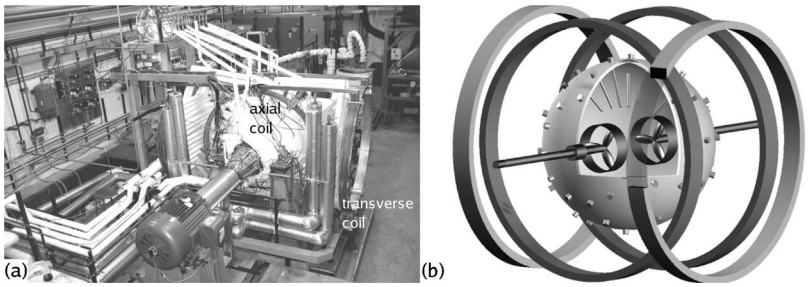

FIG. 1. (a) Photograph and (b) schematic of the Madison Dynamo Experiment. The sphere is 1 m in diameter. It is filled with 105–110 °C liquid sodium, and a flow is created by two counter-rotating impellers. Two sets of coils, one coaxial with and one transverse to the drive shafts, are used to apply various magnetic field configurations. The magnetic field induced by the flow is measured using Hall-effect sensors both on the surface of the sphere and within tubes that extend into the flow.

$\tau_\sigma = \mu_0 \sigma a^2$, where a is a characteristic size of the system. Recast in dimensionless units, the induction equation becomes

$$\frac{\partial \mathbf{B}}{\partial t} = \mathrm{Rm} \boldsymbol{\nabla} \times \mathbf{V} \times \mathbf{B} + \boldsymbol{\nabla}^2 \mathbf{B}, \tag{3}$$

where the magnetic Reynolds number $\mathrm{Rm} = \mu_0 \sigma a v_0$ is a measure of the rate of advection compared to the rate of magnetic diffusion (v_0 is a characteristic speed). The relative importance of the Lorentz force in the flow dynamics is given by the interaction parameter $N = \sigma a B_0^2 / \rho v_0$, where B_0 is a characteristic field strength. For a kinematic dynamo, $N \ll 1$ so that the velocity field evolves independently of the magnetic field. If the flow is stationary (i.e., the flow geometry is constant in time), the induction equation becomes linear in $\mathbf{B}$; it can be solved as an eigenvalue equation by expanding $\mathbf{B}$ as

$$\mathbf{B}(\mathbf{r},t) = \sum_i \mathbf{B}_i(\mathbf{r}) e^{\lambda_i t}, \tag{4}$$

where λ_i are the growth rates of the magnetic eigenmodes $\mathbf{B}_i(\mathbf{r})$. A dynamo is produced when at least one eigenvalue has a positive real growth rate.

There are two fundamental requirements for a flow to produce a dynamo. The first requirement is a sufficiently fast flow speed so that the advection of the magnetic field overcomes ohmic dissipation.[8] There is a minimum magnetic Reynolds number $\mathrm{Rm}_{\mathrm{crit}}$ below which resistive diffusion dominates the evolution of the field. As $\mathrm{Rm} \to \mathrm{Rm}_{\mathrm{crit}}$, it is expected that the flow will more effectively amplify the initial seed field to produce a dynamo. The second requirement is feedback—the induced field must reinforce the initial seed field. Although the flow may induce a strong response from an initial seed field, there is no feedback to continue the cycle of magnetic field generation if the induced field is perpendicular to the seed field.

The amplification and feedback can be quantified by the gain, defined as

$$\mathrm{gain} = \frac{B_{\mathrm{induced}} \cos \delta + B_{\mathrm{applied}}}{B_{\mathrm{applied}}}. \tag{5}$$

Here, B_{induced} is a measure of the amplitude of the induced field, B_{applied} is a measure of the amplitude of the applied field, and δ is the angle defining the relative orientation of the induced field to the applied field. The mechanism that produces a dynamo is described in terms of amplification and feedback in Sec. II B and the use of Eq. (5) in analyzing measurements from the experiment is described in Sec. IV B.

B. Experimental flow modeling

Although the impeller-generated flow in the experiment is turbulent, the mean flow can be approximated by a laminar model. Flows in a spherical geometry are most easily modeled by the Bullard and Gellman formalism.[9] The velocity field is described by a spherical harmonic expansion of toroidal and poloidal stream functions[10]

$$\mathbf{V}(r,\theta,\phi) = \sum_{\ell,m} (\boldsymbol{\nabla} \times \boldsymbol{\nabla} \times [s_{\ell,m}(r) Y_\ell^m(\theta,\phi)\hat{\mathbf{r}}] + \boldsymbol{\nabla} \times [t_{\ell,m}(r) Y_\ell^m(\theta,\phi)\hat{\mathbf{r}}]) \tag{6}$$

and the magnetic field is described by an expansion of flux functions

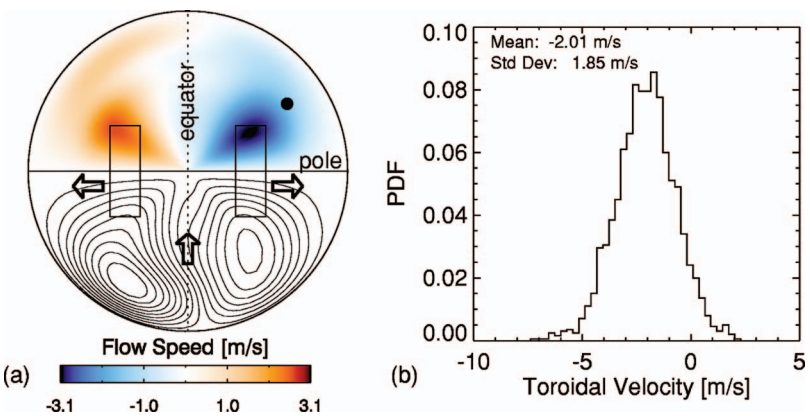

FIG. 2. (Color) (a) Velocity field profiles fitted to LDV measurements of water flows generated by impellers identical to those used in the sodium experiment. The impeller rotation rate is 16.7 Hz, corresponding to $\mathrm{Rm}_{\mathrm{tip}} = 100$ based on impeller tip speed. A contour plot of the toroidal flow is shown in the upper hemisphere, and poloidal stream lines are shown in the lower hemisphere. The poloidal flow is directed inward at the equator and outward at the poles. The two rectangles represent the location of the impellers. The $s_{1,0}$, $s_{2,0}$, $s_{4,0}$, $t_{1,0}$, $t_{2,0}$, and $t_{4,0}$ profiles are used for the flow model. (b) The probability distribution function for an LDV measurement of the toroidal velocity in the water model of the sodium experiment. The measurement location is shown as the circular dot in (a).

Downloaded 08 May 2006 to 128.104.49.126. Redistribution subject to AIP license or copyright, see http://pop.aip.org/pop/copyright.jsp

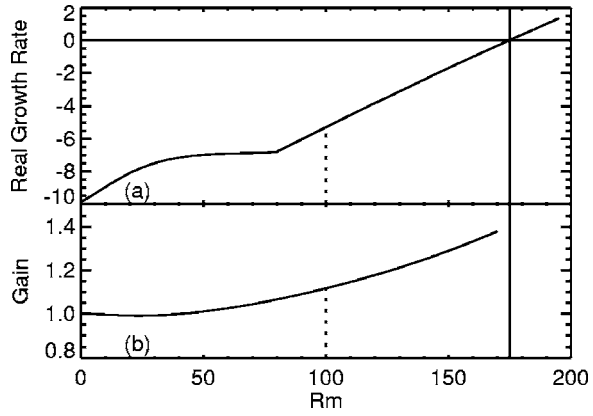

FIG. 3. (a) The kinematic growth rate of the dominant eigenmode vs Rm. The growth rate is calculated from the linearized induction equation using the flow profile constructed from LDV measurements in a water model of the sodium experiment, where $\mathrm{Rm}_{\mathrm{tip}}=100$ (Rm=98 based on maximum velocity). It is assumed that the impellers generate the same flow profile as the impeller tip speed is increased and that the maximum flow speed scales linearly with the tip speed. (b) The corresponding gain as defined in Eq. (5). The amplification of magnetic flux grows as the flow reaches $\mathrm{Rm}_{\mathrm{crit}}=175$. Above $\mathrm{Rm}_{\mathrm{crit}}$, the gain is undefined since the kinematic model does not account for the saturation of the magnetic field.

$$\mathbf{B}(r,\theta,\phi)=\sum_{\ell,m}(\boldsymbol{\nabla}\times\boldsymbol{\nabla}\times[S_{\ell,m}(r)Y_{\ell}^{m}(\theta,\phi)\hat{\mathbf{r}}]+\boldsymbol{\nabla}\times[T_{\ell,m}(r)Y_{\ell}^{m}(\theta,\phi)\hat{\mathbf{r}}]),\tag{7}$$

where the $Y_{\ell}^{m}(\theta,\phi)$ are the spherical harmonics, $s_{\ell,m}(r)$ and $t_{\ell,m}(r)$ are radial scalar profiles describing the poloidal and toroidal velocity field, and $S_{\ell,m}(r)$ and $T_{\ell,m}(r)$ are radial scalar profiles describing the poloidal and toroidal magnetic field. The experimental flow is axisymmetric and is composed of primarily the $t_{2,0}$ and $s_{2,0}$ terms. Hence, it is called a $t2s2$ flow.

The velocity field depicted in Fig. 2(a) is determined from laser Doppler velocimetry (LDV) measurements performed in an identical-scale water model of the sodium experiment.[5] Liquid sodium at 120 °C has the same kinematic viscosity and density as water at 40 °C, so the flow measured in the water model should correspond to the sodium flow. The magnitude of velocity fluctuations is extremely large, as can be seen from the probability distribution function from LDV measurements depicted in Fig. 2(b). The flow profile depicted in Fig. 2(a) is therefore only realized in a mean sense. The instantaneous flow profile can deviate significantly from the mean, implying that the eigenmode growth rate should fluctuate on the time scale of the flow evolution. The induced field would then exhibit transient behavior, especially for flows near $\mathrm{Rm}_{\mathrm{crit}}$. The autocorrelation time of the LDV measurements of the flow is $\tau_c=60\pm20$ ms for $\mathrm{Rm}_{\mathrm{tip}}=100$, which serves as an estimate of the time scale for changes in the flow profile.

An eigenmode analysis of the flow profile shown in Fig. 2(a) suggests that a magnetic field should be generated for $\mathrm{Rm}\geqslant175$ as seen in Fig. 3(a). The structure of the magnetic eigenmode with the largest growth rate for the $t2s2$ flow is dominated by the $S_{1,1}$ term in the expansion of Eq. (7), corresponding to a dipole field oriented perpendicular to the axis of symmetry of the flow (note the field lines in the first panel of Fig. 4). The gain, shown in Fig. 3(b), is calculated from Eq. (5), where B_{induced} is the strength of the transverse dipole field induced by the flow subjected to a transverse dipole field of strength B_{applied}. The azimuthal angle between the induced and applied fields is δ. It can be seen from Fig. 3(b) that the gain increases as $\mathrm{Rm}\rightarrow\mathrm{Rm}_{\mathrm{crit}}$, though the feedback is insufficient to produce a dynamo until $\mathrm{Rm}>\mathrm{Rm}_{\mathrm{crit}}$. It should also be noted that Cowling's antidynamo theorem does not apply since the eigenmode breaks the system's axisymmetry.[8]

The physical mechanism of the gain and feedback for the $t2s2$ flow is demonstrated by following the evolution of a field line in the frozen-flux approximation [the diffusion term in Eq. (3) is neglected]. In Fig. 4, two field lines parallel to the equatorial plane are stretched to the poles (located where the drive shafts enter the sphere) by the poloidal flow and twisted by the toroidal flow back into their original direction. The induced field enhances the initial seed field, thereby increasing its magnetic flux. This process continues as tension in the field lines builds. The frozen-flux assumption eventually becomes invalid; the field line tension presumably is relieved through magnetic reconnection due to resistive diffusion. Once the magnetic field becomes sufficiently strong, the interaction parameter becomes large. The Lorentz force creates a torque on the flow, referred to as the back reaction, which halts the field growth.

The laminar analysis above may be inadequate for describing the experiment since turbulence also induces magnetic fields. Eddies in the flow distort the magnetic field, creating small-scale magnetic field structures which can affect the large-scale induced field. Mean field theory suggests that velocity field fluctuations can enhance the resistivity of the fluid by effectively increasing the rate of diffusion (the β effect),[11] generate large-scale currents through helical fluid motion (the α effect),[12] and reduce the magnetic field within the flow due to inhomogeneities in the magnitude of turbulent fluctuations (the γ effect).[13] The usual assumptions of homogeneous, isotropic turbulence and scale separation of fluctuations from the mean flow are not necessarily satisfied in the experiment; hence the effects described are only used for conceptual understanding.

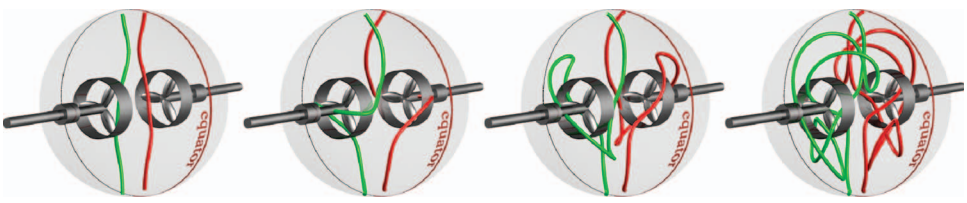

FIG. 4. (Color) The mechanism of field generation in a laminar double-vortex flow is modeled in the frozen flux limit ($\mathrm{Rm}\rightarrow\infty$). Field lines near the equatorial plane are stretched by the poloidal flow toward the pole and then twisted back onto themselves by the toroidal flow.

Downloaded 08 May 2006 to 128.104.49.126. Redistribution subject to AIP license or copyright, see http://pop.aip.org/pop/copyright.jsp

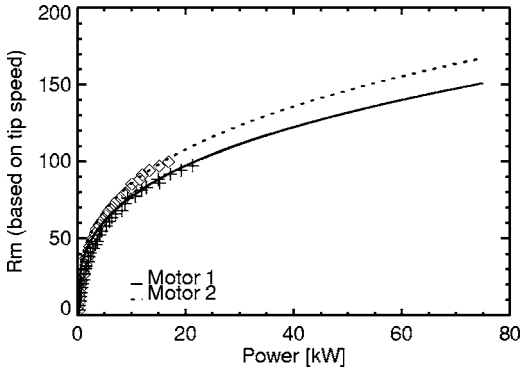

FIG. 5. The motor power follows the characteristic cubic relationship with the impeller rotation rate that is proportional to Rm. The curve is extrapolated to the maximum motor power available, yielding $\mathrm{Rm}_{\max}=150$.

III. DESCRIPTION OF THE EXPERIMENT

The experiments are performed in a 1 m diam, 1.6 cm thick stainless-steel sphere shown in Fig. 1. Liquid sodium is transferred pneumatically from a storage vessel, located in a vault beneath the floor, to the sphere using pressurized argon. The sodium fills the sphere from the bottom until the liquid level rises to an expansion tank connected to the top of the sphere. The expansion tank accommodates changes in the volume of the sodium due to variation in temperature. The weight of the sodium in the storage vessel is monitored during the transfer to determine the liquid level in the sphere. Electrical contact switches in the expansion tank provide a redundant means of determining the sodium fill level.

The conductivity of liquid sodium varies with temperature. It has a maximum value of $1.05\times10^{7}(\Omega\ \mathrm{m})^{-1}$ near the freezing point of sodium (98 °C) and decreases by about 4% for every 10 °C. Since $\mathrm{Rm}\propto\sigma$, the sphere is kept at a temperature of 105–110 °C to optimize Rm without freezing the sodium. The sphere's temperature is maintained by a heat exchange system that runs heat-transfer oil through a series of copper tubes on the sphere's surface. The system provides 12 kW of heating and 75 kW of cooling to the oil. Kaowool insulation reduces the sphere's ambient heat loss. The heat introduced to the sodium by the rotating impellers is removed through the surface of the sphere by the heat exchange system.

Two 30.5 cm diam impellers generate the flow. They are driven by 75 kW motors controlled by variable frequency drives (VFDs). The motors rotate the impellers at rates from 3–30 Hz ($\mathrm{Rm}_{\mathrm{tip}}$ is between 18 and 180). Since $\mathrm{Rm}_{\mathrm{crit}}$ depends on flow geometry, the impellers have been modified to produce the desired flow: Kört nozzles limit the radial thrust and fins on the exterior of the nozzles increase the mean toroidal flow.[5] The magnetic Reynolds number $\mathrm{Rm}_{\mathrm{tip}}$ is approximated using the rotation rate of the impellers, which is measured by digital encoders. Although convenient, this estimate is generous in that the speed of the impeller tip is much larger than that of the bulk flow. The VFDs record torque and power information. The motor power follows a cubic relationship with rotation rate as shown in Fig. 5. Once a dynamo is achieved, it is expected that the back reaction due to the Lorentz force will increase the power required to drive the impellers beyond the cubic extrapolation shown.

At atmospheric pressure, the rotating impellers cause cavitation by creating a rapid drop in the local pressure near the impeller blades, forming bubbles in the fluid. When the bubbles collapse against the blades, they emit ultrasonic noise which is monitored by a transducer mounted to the sphere. Since these bubbles disrupt the flow through the impellers, the cavitation must be suppressed. This suppression is accomplished by pressurizing the sphere with argon gas. The required pressurization is determined empirically by increasing the sphere pressure until the ultrasonic noise is minimized. For example, to operate at a rotation rate of 20 Hz, the sphere must be pressurized to 550 kPa (80 psi).

Two sets of coils generate magnetic fields used to study the inductive response of the flow. One set is coaxial with the drive shafts, the other orthogonal, as shown in Fig. 1. A dc power supply provides the coils with 600 A to generate fields up to 100 G. The coils can produce dipole, quadrupole, transverse dipole, and transverse quadrupole field configurations. For flow speeds of 10 m/s, the interaction parameter is $N=10^{-3}$; hence the magnetic field is advected passively by the flow.

The magnetic field is measured using Hall-effect probes (Analog Devices AD22 151 Linear Output Magnetic Field Sensors) on integrated circuits with internal temperature compensation. The probes saturate at ±170 G. The signals are sent through a low-pass filter to reduce the noise level. Since the sphere shields the probes from frequencies higher than the skin-effect frequency, the low-pass filter is designed to have a roll-off frequency that matches the skin-effect frequency. For the $d=1.6$ cm thick stainless-steel sphere ($\eta\sim7.2\times10^{-7}\ \Omega\ \mathrm{m}$), this frequency is $f_{\mathrm{skin}}\sim(\pi\mu_0\sigma d^2)^{-1}\sim1$ kHz. Probes are positioned on a grid on the surface of the sphere capable of resolving spherical harmonic modes up to a polar order of $\ell=7$ and an azimuthal order of $m=5$. Linear arrays of probes in stainless-steel tubes are inserted radially into the sphere and are oriented to measure either axial or toroidal magnetic fields. Data from the magnetic probes are sampled by 16-bit digitizers on PC-based data acquisition cards at a rate of 1 kHz per channel, which is sufficient to resolve fluctuations due to eddies down to the resistive dissipation scale (see Sec. V). The stainless-steel tubes encasing the internal sensor arrays vibrate when the impellers are driven at rotation rates above 15 Hz ($\mathrm{Rm}_{\mathrm{tip}}=90$). Since the amplitude of the vibrations increases with flow speed, experiments are limited to the lower rotation rates to prevent damaging the tubes and risking a breach. A comparison of data from experiments before the internal arrays were installed with data from experiments with the tubes indicates that the disturbance in the flow due to the tubes has negligible effect on the large-scale induced magnetic field. Future experiments will be performed without the internal sensor arrays to reach higher rotation rates.

Downloaded 08 May 2006 to 128.104.49.126. Redistribution subject to AIP license or copyright, see http://pop.aip.org/pop/copyright.jsp

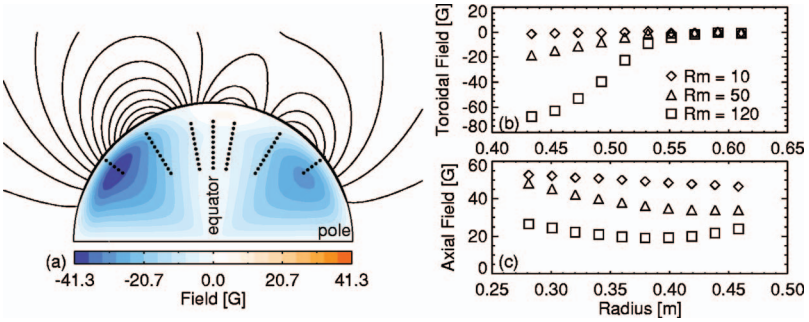

FIG. 6. (Color) (a) A plot of the toroidal magnetic field produced by the ω effect when a 60 G axial field is applied to a $t2s2$ flow with Rm=100. The contours are calculated by fitting the expected $T_{\ell,m}(r)$ profiles to measurements of the internal toroidal field. The dots indicate the position of the Hall probes. External field lines are shown based on a vacuum-field expansion fit to measurements from the surface probe array. (b) Toroidal magnetic field measurements near the toroidal maximum above the impeller and (c) axial magnetic field measurements in the equatorial plane for various Rm.

IV. MAGNETIC FIELD MEASUREMENTS

A. Reconstruction of the mean magnetic field

The induction effects are studied by applying an axial magnetic field to both flowing and stationary sodium and comparing the measured fields. The flow's differential rotation wraps the field lines around the drive shaft axis to produce a toroidal magnetic field through the so-called ω effect, as seen in Fig. 6(a). The contour plot is generated by fitting the coefficients of the harmonic expansion in Eq. (7) to toroidal field measurements (up to order $\ell=3$). The ω effect is very efficient at amplifying the applied magnetic field; measurements of the toroidal magnetic field shown in Fig. 6(b) indicate that the induced toroidal field increases with $\mathrm{Rm}_{\mathrm{tip}}$ and is larger than the applied field for $\mathrm{Rm}_{\mathrm{tip}}=120$. In contrast, Fig. 6 shows that the axial magnetic field in the equatorial plane is reduced by half. This reduction of poloidal magnetic flux can be explained by the effect of flux expulsion due to the strong poloidal circulation in the $t2s2$ flow.[8]

The mean field structure shown in Fig. 6(a) is obtained by an averaging procedure which calculates the peak of the histogram of magnetic field measurements from each probe. This technique is necessary since some of the signals have non-Gaussian statistics (discussed in Sec. V). The resulting mean field is predominantly due to odd harmonics in accordance with the selection rules governing the interaction terms of the induction equation.[9]

The magnetic field outside the sphere is reconstructed from the field harmonics calculated from the surface array measurements. The poloidal flux lines are shown in Fig. 6(a). Since the Hall probes on the surface of the sphere lie outside regions containing currents, the measured field can be described in terms of a vacuum field potential that satisfies $\nabla^2\Phi=0$, where $\mathbf{B}=-\boldsymbol{\nabla}\Phi$. Solving Laplace's equation for the potential in a spherical geometry yields

$$\Phi(r,\theta,\phi)=\sum_{\ell,m}\left(C_{\ell,m}r^{\ell}+\frac{D_{\ell,m}}{r^{\ell+1}}\right)Y_{\ell}^{m}(\theta,\phi). \tag{8}$$

The $C_{\ell,m}$ terms are due to currents in the external field coils whereas the $D_{\ell,m}$ terms are due to currents in the flow. The field can be separated into applied and induced fields whose radial components are

$$\mathbf{B}_{\mathrm{applied}}\cdot\hat{\boldsymbol{r}}=-\sum_{\ell,m}C_{\ell,m}r^{\ell-1}\,\ell\,Y_{\ell}^{m}(\theta,\phi), \tag{9}$$

$$\mathbf{B}_{\mathrm{induced}}\cdot\hat{\boldsymbol{r}}=\sum_{\ell,m}\frac{D_{\ell,m}}{r^{\ell+2}}(\ell+1)Y_{\ell}^{m}(\theta,\phi). \tag{10}$$

The external measured magnetic field can be completely described in terms of these expansion coefficients. To determine the coefficients $D_{\ell,m}$ for a given set of magnetic field measurements, the applied field is subtracted from the measured field, and a design matrix A_{ij} is constructed that satisfies $\mathsf{B}_i=\mathsf{A}_{ij}\mathsf{D}_j$, where $\mathsf{B}_i=B_r(r_i,\theta_i,\phi_i)$ is an array of measurements of the induced field and $\mathsf{D}_j=D_{\ell_j,m_j}$ is the array of expansion coefficients in Eq. (10). An example of an element of the design matrix is

$$A_{i,j}=\left(\frac{\ell_j+1}{r_i^{\ell_j+2}}\right)Y_{\ell_j}^{m_j}(\theta_i,\phi_i). \tag{11}$$

The coefficients are obtained by matrix inversion using singular value decomposition[14] to solve $\mathsf{D}_j=(\mathsf{A}_{ij})^{-1}\mathsf{B}_i$. Axisymmetric mode time series are shown in Fig. 7, where the modes have been evaluated at $\theta=0$. The dipole component of the induced magnetic field grows nonlinearly with $\mathrm{Rm}_{\mathrm{tip}}$ and cannot be explained by induction effects from an axisymmetric flow. The dipole response results from a turbulent electromagnetic force (EMF) generated by correlated turbulent fluctuations in the flow.[15]

B. Measuring gain with a transverse applied field

The proximity of the flow to magnetic self-excitation is studied by applying a magnetic field perpendicular to the

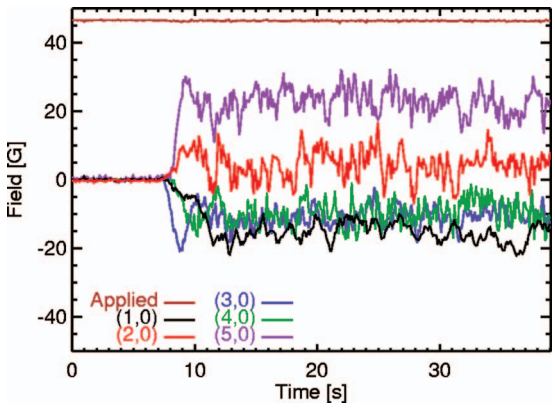

FIG. 7. (Color) Time series plots of the axisymmetric modes evaluated at $\theta=0$. A constant external dipole field is applied and the motors are turned on at $t=7$ s.

Downloaded 08 May 2006 to 128.104.49.126. Redistribution subject to AIP license or copyright, see http://pop.aip.org/pop/copyright.jsp

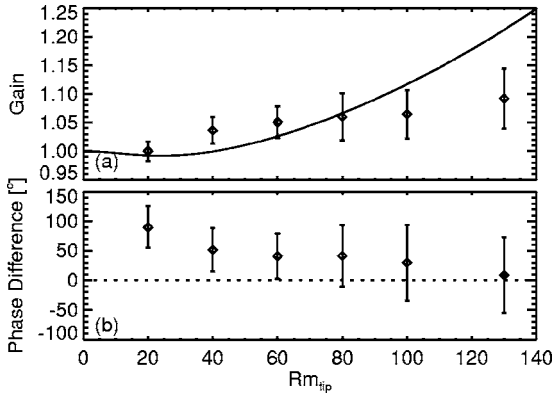

FIG. 8. (a) Amplification of a magnetic field applied perpendicular to the drive shaft axis as a function of Rm_{tip}. Gain is defined in Eq. (5). The solid line is the gain predicted by the kinematic model shown in Fig. 3(b). (b) Azimuthal angle between the induced transverse dipole field and the applied field. Error bars on both plots indicate rms fluctuation levels.

drive shaft axis. Recall from Sec. II that the anticipated structure of the magnetic field generated by the dynamo is a dipole oriented in this direction. Figure 3(b) suggests that such a field should be amplified by the flow. As in Sec. II, the gain in Eq. (5) is calculated using the $\ell=1$, $m=1$ expansion term in Eq. (10) for B_{induced}, and δ is the azimuthal angle between the applied and induced fields. The gain is less than one if a component of the induced field is antiparallel to the applied field, indicating attenuation, and is greater than one if the fields are in phase. The gain is determined from measurements of the induced magnetic field and is shown to increase with Rm_{tip} in Fig. 8(a), though not as quickly as anticipated from the kinematic model. Figure 8(b) shows that the induced field is somewhat out of phase with the applied field at low Rm_{tip} and that the alignment improves as Rm_{tip} increases. These measurements will be used to obtain a flow profile in the sodium experiment that maximizes the gain.

V. PROPERTIES OF MHD TURBULENCE

The preceding analysis documents the large-scale induced mean field. Since the flow is turbulent with $Rm \gg 1$ and the magnetic field is relatively weak, eddies can twist and stretch field lines at many scales. While smaller eddies are advected by the mean flow, larger eddies can distort the large-scale flow itself and cause intermittent behavior in the induced field.[16] Figure 9 shows signals from two Hall probes on the surface of the sphere and their probability distribution functions (PDFs). In addition to random fluctuations with a Gaussian distribution, the Hall probe signal in Fig. 9(a) has large-amplitude bursts that skew its PDF shown in Fig. 9(b). The time average of the signal for this probe is therefore not the most-probable value of the field. The signal shown in Fig. 9(c) from a probe near one of the drive shafts, however, has normal statistics. Examination of the structure of the magnetic field during the bursts reveals a strong $m=1$ mode shown in Fig. 10. The turbulent flow thus induces an axisymmetric field on average punctuated by intermittent bursts that break the symmetry.

Eddies at the smaller scales create structure in the magnetic field down to the viscous dissipation scale.[17] This structure is evident in the spatial spectrum in Fig. 11. The spatial spectrum is constructed from the power spectrum of the signal from a Hall probe that measures the toroidal field just above one of the impellers. The two power-law scalings shown in Fig. 11 can be derived from the induction equation using a weak-field approximation. The magnetic field is described in terms of a mean and a weak fluctuating part, $\mathbf{B}=\mathbf{B}_0+\tilde{\mathbf{B}}$. The Fourier transform of Eq. (3) becomes

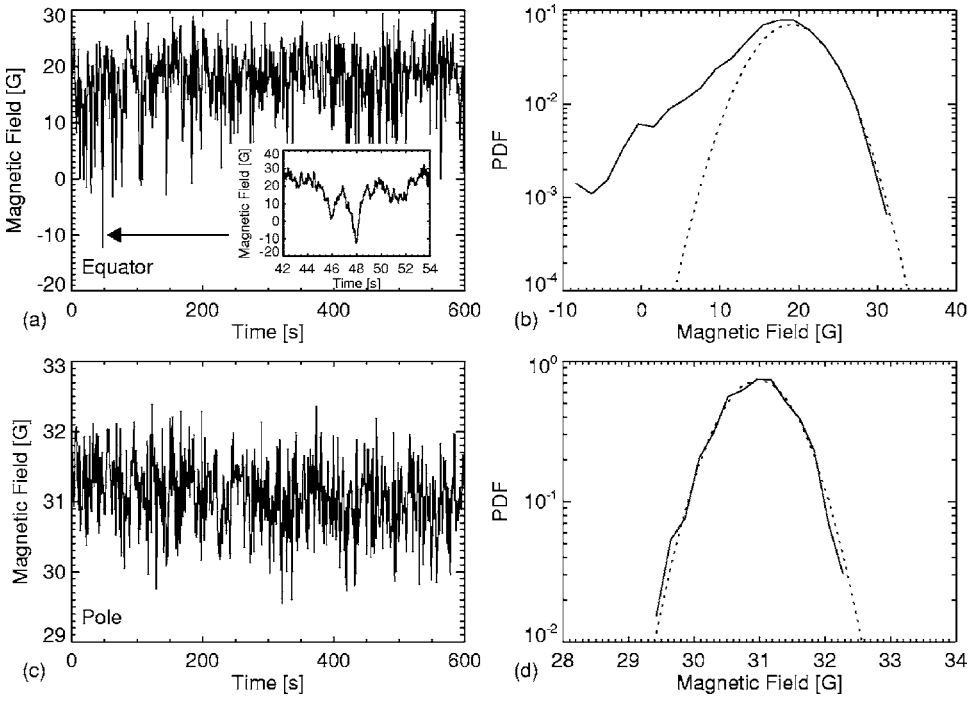

FIG. 9. (a) Measurement from a single Hall probe on the surface of the sphere near the equator. (b) The probability distribution for the signal in (a). The impeller rotation rate for this example is 16.7 Hz (Rm=100) and a 60 G dipole field is applied. A Gaussian fit to the right side of the distribution is shown (dotted line) to illustrate the asymmetry. (c) The time series from a probe near the drive shaft axis (or pole) and (d) its probability distribution is shown for comparison.

Downloaded 08 May 2006 to 128.104.49.126. Redistribution subject to AIP license or copyright, see http://pop.aip.org/pop/copyright.jsp

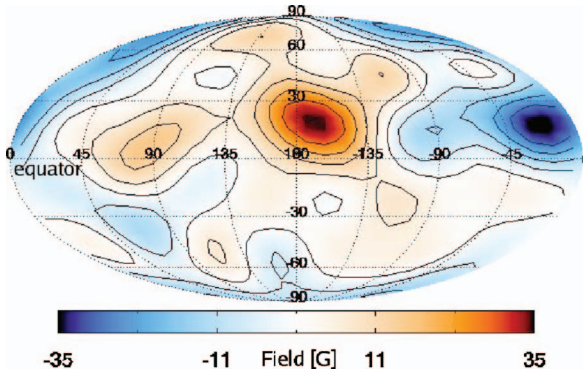

FIG. 10. (Color) The mode structure of the intermittent bursts corresponds to a dipole field aligned perpendicular to the drive shaft axis, as seen from the surface magnetic field (the axis of rotation is vertical). The mean magnetic field has been removed to isolate the structure of the fluctuation.

$$\left(i\omega + \frac{k^2}{\mu_0\sigma}\right)\tilde{\mathbf{B}}_{\mathbf{k},\omega} = i\mathbf{k} \times \mathbf{v}_{\mathbf{k},\omega} \times \mathbf{B}_0, \tag{12}$$

where second-order advection terms have been assumed to be negligible due to the weak-field approximation. Magnetic fluctuations are due primarily to the advection of eddies by the mean flow (the Taylor hypothesis[18]) and so the dispersion relation is approximately $\omega(k) \sim k v_0$. Dividing Eq. (12) by this dispersion relation gives

$$\left(\frac{i\omega}{kv_0} + \frac{k}{\mu_0\sigma v_0}\right)\tilde{\mathbf{B}}_{\mathbf{k},\omega} = i\frac{\mathbf{k}}{k} \times \frac{\mathbf{v}_{\mathbf{k},\omega}}{v_0} \times \mathbf{B}_0. \tag{13}$$

At scales $k \ll k_\sigma \equiv \mu_0\sigma v_0 = \mathrm{Rm}/a$, the dissipation term is small. Thus, magnetic fluctuations at these scales are primarily due to advection of the mean field by velocity fluctuations, giving $\tilde{B}^2_{k,\omega}/B_0^2 \sim v^2_{k,\omega}/v_0^2$. For isotropic, homogeneous turbulence, the velocity spectrum is the Kolmogorov spectrum $E_K(k) = v^2_{k,\omega}/k \propto k^{-5/3}$. The resulting magnetic spectrum is $E_M(k) = \tilde{B}^2_{k,\omega}/k \propto k^{-5/3}$, as seen in Fig. 11 for the range

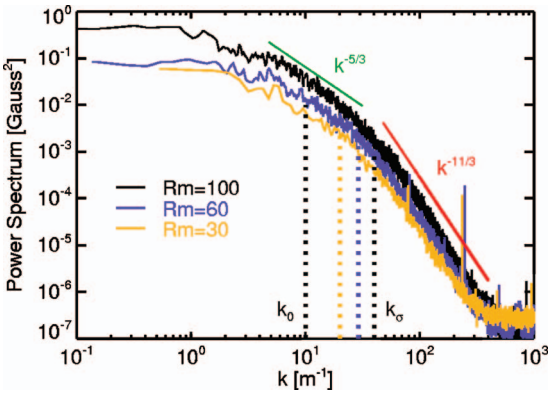

FIG. 11. (Color) The inferred spatial spectrum constructed from the Fourier transform of the signal from a Hall probe inside the sphere for three different values of $\mathrm{Rm}_{\mathrm{tip}}$. The probe is located just above the impeller near the toroidal maximum in Fig. 6. Fluctuations are assumed to be due to convection of spatial variations in the field. The dispersion relation is $\omega = k v_0$, where v_0 is determined from velocity measurements in the water model of the sodium experiment. The wave number corresponding to the scale size of the experiment is labeled as k_0. The wave number corresponding to the dissipation scale k_σ is labeled for the three spectra.

TABLE I. The resistive dissipation scale determined from the spatial spectrum in Fig. 11. The velocity is measured in the water model of the experiment at the probe's position.

$\mathrm{Rm}_{\mathrm{tip}}$	v_0 (m/s)	k_σ (m^{-1})
30	0.39	20
60	0.78	29
100	1.2	40

$k_0 < k < k_\sigma$. This scaling was observed in the Maryland Dynamo Experiment,[19] but in the von Kármán sodium (VKS) experiment, a k^{-1} scaling was observed.[7] The discrepancy was attributed to a saturation of the induction mechanism.

For the range $k \gg k_\sigma$, the diffusion term in Eq. (13) becomes large. Balancing this term with the right-hand side yields the scaling $\tilde{B}^2_{k,\omega}/B_0^2 \sim (\mu_0\sigma/k)^2 v^2_{k,\omega}$. Hence, the magnetic spectrum is $E_M(k) \propto k^{-2} E_K(k) \propto k^{-11/3}$ in the resistive dissipation range, as seen in Fig. 11 for $k > k_\sigma$. The $k^{-11/3}$ scaling was observed in the VKS experiment, but the Maryland experiment observed a steeper spectrum due to shielding effects of the stainless-steel vessel.

The dissipation scale k_σ is evident from the knee in the wave-number spectrum of Fig. 11. The results are summarized in Table I, showing that k_σ increases with $\mathrm{Rm}_{\mathrm{tip}}$. Consequently, the magnetic field gains structure at smaller scales as $\mathrm{Rm}_{\mathrm{tip}}$ increases, down to scale sizes of $\ell_\sigma = 2\pi/k_\sigma = 16$ cm at $\mathrm{Rm}_{\mathrm{tip}} = 100$. A magnetic Reynolds number for the turbulent part of the flow can be constructed assuming that $k_\sigma = \mathrm{Rm}_{\mathrm{turb}} k_0$. Using the values in Table I, it can be shown that $\mathrm{Rm}_{\mathrm{turb}} = 0.2\mathrm{Rm}_{\mathrm{tip}}$. This relation implies that the small-scale turbulent eddies produced by the mean flow are slower than the injection-scale eddies. The dissipation scale is therefore only about one decade smaller than the injection scale rather than the two decades expected for a flow with $\mathrm{Rm} \sim 100$. As a result, the small-scale dynamics of the flow has little role in generating magnetic fields; it is the largest eddies in the flow that induce magnetic fields and that have the greatest impact on the transition to a dynamo.

VI. CONCLUSION

The magnetic field induced by a turbulent flow of liquid sodium demonstrates flux expulsion and the ω effect. The flow generated in the experiment induces a field that provides amplification and feedback, the necessary ingredients of a dynamo. Power spectrum measurements show that the resistive dissipation scale is inversely proportional to Rm. The turbulent flow creates intermittent bursts of large-scale magnetic fields that have a structure similar to the magnetic field predicted from the laminar kinematic dynamo model. Consequently, as a flow nears $\mathrm{Rm}_{\mathrm{crit}}$, the transition to a dynamo appears to be intermittent rather than smooth.

ACKNOWLEDGMENTS

Special thanks go to C. A. Parada, B. A. Grierson, and M. Fix for their aid in constructing the experiment and to R. A. Bayliss for helpful conversations.

Downloaded 08 May 2006 to 128.104.49.126. Redistribution subject to AIP license or copyright, see http://pop.aip.org/pop/copyright.jsp

The authors would like to acknowledge the generous financial support for this project from the Department of Energy, the National Science Foundation, the Packard and Sloan Foundations, and the Research Corporation.

[1] R. Stieglitz and U. Müller, Phys. Fluids **13**, 561 (2001).
[2] A. Gailitis, O. Lielausis, S. Dementév *et al.*, Phys. Rev. Lett. **84**, 4365 (2000).
[3] M. L. Dudley and R. W. James, Proc. R. Soc. London, Ser. A **425**, 407 (1989).
[4] R. O'Connell, R. Kendrick, M. Nornberg, E. Spence, A. Bayliss, and C. B. Forest, "On the Possibility of an Homogeneous MHD Dynamo in the Laboratory," in *Dynamo And Dynamics, A Mathematical Challenge*, edited by P. Chossat, D. Ambruster, and I. Oprea, Vol. 26 of NATO Science Series II, Mathematics, Physics and Chemistry (NATO Science Programme, Kluwer Academic, Dordrecht, 2000), pp. 59–66.
[5] C. B. Forest, R. A. Bayliss, R. D. Kendrick, M. D. Nornberg, R. O'Connell, and E. J. Spence, Magnetohydrodynamics **38**, 107 (2002).
[6] D. P. Lathrop, W. L. Shew, and D. R. Sisan, Plasma Phys. Controlled Fusion **43**, A151 (2001).
[7] M. Bourgoin, L. Marié, F. Pétrélis *et al.*, Phys. Plasmas **14**, 3046 (2002).
[8] H. K. Moffatt, *Magnetic Field Generation in Electrically Conducting Fluids* (Cambridge University Press, Cambridge, 1978).
[9] E. C. Bullard and H. Gellman, Philos. Trans. R. Soc. London, Ser. A **247**, 213 (1954).
[10] In a spherical geometry, toroidal field lines are confined to spherical surfaces whereas poloidal field lines penetrate spherical surfaces.
[11] A. B. Reighard and M. R. Brown, Phys. Rev. Lett. **86**, 2794 (2001).
[12] E. N. Parker, Astrophys. J. **122**, 293 (1955).
[13] K. Krause and K. H. Rädler, *Mean-field Magnetohydrodynamics and Dynamo Theory* (Pergamon, New York, 1980).
[14] W. H. Press, S. A. Teukolsky, W. T. Vetterling, and B. P. Flannery, *Numerical Recipes in C: The Art of Scientific Computing*, 2nd ed. (Cambridge University Press, Cambridge, 2002).
[15] E. J. Spence, M. D. Nornberg, C. M. Jacobson, R. D. Kendrick, and C. B. Forest, Phys. Rev. Lett. **96**, 055002 (2006).
[16] H. Tennekes and J. L. Lumley, *A First Course in Turbulence* (MIT, Cambridge, MA, 1972).
[17] R. H. Kraichnan and S. Nagarajan, Phys. Fluids **10**, 859 (1967).
[18] G. I. Taylor, Proc. R. Soc. London, Ser. A **164**, 476 (1938).
[19] N. L. Peffley, A. B. Cawthorne, and D. P. Lathrop, Phys. Rev. E **61**, 5287 (2000).

Downloaded 08 May 2006 to 128.104.49.126. Redistribution subject to AIP license or copyright, see http://pop.aip.org/pop/copyright.jsp